Network Volatility in Emerging Markets: A Factor-Adjusted Stochastic Volatility Analysis of Brazil's Equity Dynamics

João Pedro M. Franco[†]
Márcio P. Laurini[‡]

Abstract

This study investigates volatility interdependencies in Brazil's equity market using Factor-Adjusted Networks (FNETS) built from latent volatilities estimated via Stochastic Volatility (SV) models. Analyzing companies from the Bovespa Theoretical Portfolio between January and April 2025, over the period 2022–2025, we uncover heterogeneous network structures: core stocks exhibit strong systemic linkages, while peripheral firms display weaker connections. Methodologically, FNETS captures Granger-causal, contemporaneous, and long-run dependencies, while the SV model outperforms traditional OHLC/HL volatility measures, yielding lower forecasting errors. The findings enhance systemic risk monitoring and offer actionable insights for policymakers and investors in emerging markets.

Keywords: Volatility spillovers, factor-adjusted networks, stochastic volatility, systemic risk, Brazilian equity market.
JEL Code:

1. Introduction

Financial crises are recurrent phenomena with striking similarities, often characterized by sudden surges in market volatility and cross-border spillovers that amplify systemic risk. During such episodes, volatility not only intensifies within the originating assets but also propagates across markets, highlighting the importance of quantifying spillover dynamics for early crisis detection and real-time monitoring (Yilmaz, 2010; Diebold and Yilmaz, 2012; Diebold and Yılmaz, 2014).

The global financial crisis of 2007–2008, for instance, exposed the vulnerabilities of interconnected markets and the cascading effects of volatility, underscoring the need for robust risk management frameworks (Zhang et al., 2018). In emerging economies understanding spillover mechanisms is particularly crucial, as external shocks can destabilize domestic stability and hinder economic growth.

Submitted on February 8, 2023. Revised on May 25, 2023. Accepted on June 9, 2023. Published online in June 2023. Editor in charge: Mr Editor.

[†]Department of Economics - FEARP USP: joaopfranco@usp.br
[‡]Department of Economics - FEARP USP: laurini@fearp.usp.br

Financial spillover methodologies aim to quantify how shocks propagate across assets, markets, or economies using various econometric techniques. Traditional approaches, such as the Diebold-Yilmaz connectedness framework (Diebold and Yilmaz, 2009), rely on variance decomposition from vector autoregressions (VAR) to estimate spillover effects. These methods analyze how forecast errors in one asset or market can be attributed to others, providing directional spillover measures. However, they often struggle in high-dimensional settings and may overlook complex dependencies.

Network-based approaches offer an alternative by representing financial interdependencies through nodes (assets, markets) and edges (spillover effects). Techniques such as Granger causality networks, tail dependence structures, and graphical models capture systemic risk transmission, although they often require strong assumptions on structural relationships. More recent high-dimensional models, such as Fnets (Barigozzi et al., 2024), integrate dynamic latent factors to capture both contemporaneous and lagged interdependencies.

By employing sparse VAR regularization, Fnets mitigates the curse of dimensionality, enabling analysis even when the number of assets exceeds observations. Additionally, it disentangles different spillover channels, such as Granger causality and long-run dependencies, providing a more comprehensive framework for financial spillovers. These modern approaches improve upon traditional methods by enhancing real-time risk assessment in interconnected financial markets. Fnets integrates dynamic latent factor adjustment, capturing both contemporaneous and lagged interdependencies across series – features that static or variance decomposition-based methods often underestimate (Barigozzi et al., 2024).

According to Barigozzi et al. (2024), the sparse VAR regularization in Fnets, implemented via Yule-Walker equations, mitigates the curse of dimensionality, allowing for robust analysis even when the number of assets (p) exceeds the number of observations (n). Additionally, Fnets disentangles Granger causality networks, contemporaneous correlations, and long-run dependencies within a unified framework, whereas conventional methods typically focus on a single dimension. As demonstrated in Barigozzi et al. (2024), its joint forecasting capability – capturing both common and idiosyncratic components – outperforms univariate and static factor-based approaches. Moreover, Fnets proves particularly effective for data exhibiting strong cross-sectional correlations, temporal persistence, and latent network structures, all of which are key characteristics of modern financial markets.

Despite these advances in Fnets approach, existing volatility measures face limitations, since true volatility is not observable (latent). For example, Barigozzi et al. (2024) applies a very simple measure, called High-Low volatility and proposed by Parkinson (1980), to measure volatility before construct the volatility networks through Fnets method. The estimation process proposed by Garman and Klass (1980) and based on high, low, opening and closing prices, although still simple, is also widely used in the literature (Yilmaz, 2010; Diebold and Yilmaz, 2011, 2012, 2015; Cotter et al., 2023; Korobilis and Yilmaz, 2018; Demirer et al., 2018; Bostanci and Yilmaz, 2020; Demirer et al., 2019).

The Garman and Klass (1980) volatility estimator, while more efficient than close-to-close methods, has several limitations that can affect its accuracy. One key issue is its sensitivity to market microstructure noise and price jumps, as it assumes a continuous price process (Hansen and Lunde, 2006). Additionally, it does not account for overnight returns, which can lead to underestimation of total volatility when significant price movements occur outside regular trading hours. Another limitation arises from its assumption of zero drift in the price process, which may introduce bias in trending markets. The estimator also depends on intraday high and low prices, making it less effective for assets with irregular trading hours or lower liquidity. Moreover, it does not explicitly handle time-varying volatility dynamics, limiting its ability to capture volatility clustering observed in financial markets. Given these shortcomings, more advanced methods, such as stochastic volatility models or realized volatility estimators, are often preferred for robust financial analysis.

To address the challenges associated with volatility estimation and to ensure a robust analysis before constructing the volatility network, we utilize Univariate Stochastic Volatility (SV) models implemented through Integrated Nested Laplace Approximations (INLA). This Bayesian approach offers several advantages over traditional Markov Chain Monte Carlo (MCMC) methods, primarily by significantly accelerating the estimation process while maintaining a high level of accuracy (Rue et al., 2009; Simpson et al., 2017; Niekerk et al., 2019).

INLA is particularly beneficial in high-dimensional settings, where computational efficiency is crucial. It achieves this by approximating the posterior distributions of the model parameters using deterministic methods, thereby reducing the computational burden often associated with MCMC. Additionally, the flexibility of the SV models allows us to capture the underlying dynamics of volatility more effectively, accommodating features such as volatility clustering and time-varying variances that are prevalent in financial markets. By combining INLA with SV models, we can obtain precise volatility estimates that are essential for the accurate construction and analysis of the volatility network, ultimately enhancing our understanding of the interconnections among financial assets.

Our synthesis of FNETS and INLA-SV enables robust analysis of Brazil's equity market, capturing localized transmission channels. For comparison proposes, we confront the volatility forecast measured based on Fnets using SV model with the Open-High-Low-Close (OHLC) measure, as introduced by Garman and Klass (1980), and the High-Low (HL) measure, proposed by Parkinson (1980).

To verify the empirical properties of the proposed methodology we analyzed data from the Brazilian financial market. The Brazilian market, characterized by its pronounced volatility and integration with global financial networks, provides a unique landscape to explore these dynamics. By examining the relationships between different volatility measures, we aim to uncover the underlying structures that drive market behavior, including the influence of external shocks and domestic economic conditions. This approach not only enhances our comprehension of the Brazilian market but also offers insights that can be generalized to other emerging economies facing similar challenges.

We propose a comprehensive investigation into the interconnectivity among various volatility measures within a theoretical portfolio based on the Bovespa Index (Ibovespa). This analysis not only focuses on the Brazilian market but also serves as a case study with broader applications for emerging markets, where understanding volatility and its interdependencies is essential for effective risk management and investment strategies.

Our network analysis reveals heterogeneous connectivity patterns: core constituents of the portfolio exhibit strong contemporaneous and long-run linkages, while peripheral firms demonstrate weaker interdependencies. Moreover, our results highlight the superiority of Stochastic Volatility (SV) models over traditional Open-High-Low-Close (OHLC) and High-Low (HL) methods, as evidenced by significantly lower forecasting errors across multiple metrics, including Mean Absolute Error (MAE), Mean Absolute Percentage Error (MAPE), and Mean Squared Error (MSE). These insights enhance the tools available for crisis monitoring by policymakers and refine risk management strategies for investors navigating the volatile landscape of Brazil's markets.

Our contributions are threefold. Methodologically, we pioneer the integration of FNETS and SV-INLA, facilitating scalable analysis of high-dimensional stochastic systems. Empirically, we present a detailed mapping of Brazil's equity volatility network, identifying systemic nodes and fragile peripheries that are critical for understanding market stability. Practically, the precision of the SV model in forecasting volatility, as validated across various error metrics, enhances real-time crisis monitoring and portfolio hedging strategies for emerging markets, effectively addressing a significant gap in current risk management frameworks.

The remainder of this paper proceeds as follows. Section 2 details the methodology, including univariate Stochastic Volatility (SV) model estimation and FNETS implementation. Section 3 presents empirical results, emphasizing network structures. Section 4 discusses the forecasting performance and validates robustness through comparative error analysis. Section 5 concludes with policy implications and future research directions.

2. Methodology and Data

2.1 Stochastic Volatility Model

To estimate the volatility structure of an asset within a non-deterministic framework, as opposed to the deterministic nature of ARCH and GARCH models, Taylor (1982) introduces the Stochastic Volatility (SV) model. This model can be expressed in its univariate form as follows:

$$y_t = \exp\{h_t/2\}\varepsilon_t, \quad \varepsilon_t \sim \text{i.i.d. } \mathcal{N}(0,1), \tag{1}$$

$$h_t = \mu + \phi(h_{t-1} - \mu) + \eta_t, \quad \eta_t \sim \text{i.i.d. } \mathcal{N}(0, \sigma_\eta^2) \tag{2}$$

here, y_t denotes the observed return, while h_t represents the latent volatility process, which follows an autoregressive model of order 1 (AR(1)). This model is characterized by a long-term average μ and a persistence parameter $|\phi| < 1$, ensuring stationarity.

As there is no analytical solution for estimating the Stochastic Volatility (SV) model due to the intractability of the likelihood and posterior distribution (Shapovalova, 2021), the most commonly used approach for parameter estimation in SV models is Markov Chain Monte Carlo (MCMC). However, as extensively reported in the literature, this method faces convergence issues when the components of the latent volatility h_t are highly correlated. Additionally, MCMC is often inefficient in terms of computation time (Martino, 2007; Rue et al., 2009; Nacinben and Laurini, 2024).

Therefore, in this paper, we adopt an alternative Bayesian estimation method: Integrated Nested Laplace Approximations (INLA). This relatively new technique, proposed by Rue et al. (2009), enables faster computational estimation by utilizing analytical calculations rather than relying solely on Bayesian simulation methods like MCMC. The process of estimating the INLA method is described in the following section.

2.2 Integrated Nested Laplace Approximation (INLA)

As a Bayesian estimation process that has attracted attention since its formulation by Rue et al. (2009), the Integrated Nested Laplace Approximations (INLA) makes possible to speed up computational estimation time by using analytical calculations instead of Bayesian simulation methods, as Monte Carlo Markov Chain Methods (MCMC), and also avoiding the chain convergence problems associated with these procedures.

However, this property works only for models that can be rewritten (or even approximated) as Gaussian Markov Random Field (GMRF), which is a Gaussian random variable $\boldsymbol{x} = (x_1, \ldots, x_n)$, that present Markov properties, i.e., x_i and x_j, where $i \neq js$, are independent conditional on $\boldsymbol{x}_{-ij}$ (Rue et al., 2009). These Markov properties allow that, in the cases where x_i and x_j are independent conditional on $\boldsymbol{x}_{-ij}$, the corresponding entries of the precision matrix $\boldsymbol{Q}$ (inverse of the covariance matrix) are zero, $Q_{ij} = 0$.

As highlighted in Rue and Held (2005), the computational advantage occurs due to the sparsity of the precision matrix $\boldsymbol{Q}$, which has only $\mathscr{O}(n)$ of the n entries non-zero. This property allows for fast Cholesky decomposition of $\boldsymbol{Q} = \boldsymbol{L}\boldsymbol{L}^T$, where only the non-zero entries in $\boldsymbol{L}$ are calculated. For more details on Gaussian Markov Random Fields see properties (Rue and Held, 2005) or (Rue et al., 2009).

The process of estimating the SV model using the INLA approach was presented by Martino et al. (2011) and can be described as follows:

$$y|h,\theta_1 \sim \prod_{i \in \mathscr{P}} \pi(y_i|h_i,\theta_1), \tag{3}$$

$$h|\theta_2 \sim \mathscr{N}(\mu(\theta_2), Q^{-1}(\theta_2)), \tag{4}$$

where y_t represents the return and h_t denotes the log-variance, which is a latent variable. The volatility of the asset can be obtained by $\sigma_t = \exp(h_t/2)$. The vector θ_1 represents the parameters in the distribution for ε_t and vector θ_2 denotes the parameters ϕ and $\tau_h = 1/\sigma_\eta^2$, which represents the marginal precision of h_t.

Thus, the posterior distribution of the parameters $\boldsymbol{\theta} = \{\theta_1, \theta_2\}$ and the latent process h_t can be calculated as follows:

$$p(h,\theta|y) \propto p(\theta)p(h|\theta)\prod_{t=1}^{T} p(y_t|h_t,\theta). \tag{5}$$

Rue et al. (2009) argues that the INLA approach relies on the local Gaussian approximation, which can be used for inference on marginals of $p(x|y,\theta)$

that produces accurate approximations for $p(x|\theta)$ and $p(\theta_j|y)$. The densities can be computed as

$$p(x|y,\theta) \propto \exp\left(-\frac{1}{2}x^T Qx + \sum g_t(h_t)\right), \tag{6}$$

where $x = (\mu, h)$ and $g_t(h_t) = \log p(y_t|h_t, \theta)$.

According to Martino et al. (2011), a Gaussian approximation for $p(x|y,\theta)$ can be found by matching the mode, calculated iteratively using a Newton–Raphson algorithm, and the curvature at the mode. The Gaussian approximation can be described as follows:

$$\tilde{p}_G(x|y,\theta) = K_1 \exp\left(-\frac{1}{2}(x-m)^T (Q + \mathrm{diag}(c))(x-m)\right) \tag{7}$$

where K_1 denotes a normalizing constant, m denotes the modal value of the density $p(x|y,\theta)$, c represents the vector of the second-order terms in the Taylor expansion of the $\sum g_t(h_t)$ at the modal value, and Q represents the precision matrix as

$$Q = \begin{bmatrix} 1 & -\phi & & & \\ -\phi & 1+\phi^2 & -\phi & & \\ & \ddots & \ddots & \ddots & \\ & & -\phi & 1+\phi^2 & -\phi \\ & & & -\phi & 1 \end{bmatrix}. \tag{8}$$

Now, through the following steps, we can construct the approximations for $p(x_t|y)$:

1. Approximating $p(\theta|y)$

   In order to approximate the joint distribution of the hyperparameters, $p(\theta|y)$, Rue et al. (2009) proposes using the following relation:

$$\tilde{p}(\theta|y) \propto \left.\frac{p(y|x,\theta)p(x|\theta)p(\theta)}{\tilde{p}_G(x|\theta,y)}\right|_{x=m(\theta)} \tag{9}$$

   where $m(\theta)$ is the mode of $p(x|y,\theta)$.

2. Approximating $p(x_t|\theta,y)$

   Due to the high degree of complexity of the approximation of the marginals $\tilde{p}_G(x_t|\theta,y)$ in SV models, Rue et al. (2009) employs a simplified Laplace approximation, which uses the terms of the Taylor expansion to solve the problem. This approximation is given by:

$$\log\tilde{p}_{SLA}(x_t|\theta,y) = \text{const.} - \frac{1}{2}x_t^2 + \gamma_t^{(1)}(\theta)x_t + \frac{1}{6}x_t^3\gamma_t^{(3)}(\theta) + \ldots, \quad (10)$$

   where $\gamma_t^{(1)}$ and $\gamma_t^{(3)}$ capture first and third derivatives. According to Martino et al. (2011), $\gamma_t^{(3)}$ contributes to the asymmetry, while the adjustment to the mean comes from $\gamma_t^{(1)}$.

3. Numerical Integration

   Once we have the approximations for $p(\theta|y)$ and $p(x_t|\theta,y)$, the final step is a numerical integration over the hyperparameters vector, $\boldsymbol{\theta}$, using a grid of points for k. In this way, the density $p(x_t|y)$ can be approximated as

$$\tilde{p}(x_t|y) = \sum_k \tilde{p}(x_t|\theta^k,y)\tilde{p}(\theta^k|y)\Delta_k. \quad (11)$$

   where the integral is over values of θ with area-weights k. The grid points θ^k form a discrete subset of the hyperparameter space θ, strategically positioned to cover regions of high posterior density in the joint distribution $\pi(\theta|y)$.

The computational advantages of estimating SV models are studied in Ehlers and Zevallos (2015). Generalizations to long-memory processes are presented in Chaim and Laurini (2024), and to the threshold effects in de Zea Bermudez et al. (2024). Multifactor and multivariate extensions are proposed in Nacinben and Laurini (2024) and Laurini et al. (2024), indicating gains over alternative multivariate specifications.

2.3 Factor-Adjusted Vector Autoregressive Model

Factor-Adjusted Network Estimation and Forecasting (FNETS), proposed by Barigozzi et al. (2024), is a methodology designed to analyze and predict high-dimensional time series by integrating factor models with network structures. The central idea behind FNETS is to separate common latent factors from the idiosyncratic components of a multivariate time series, thereby isolating the underlying dynamic network relationships among variables. This factor-adjustment step is crucial in financial and economic applications, where strong cross-sectional dependencies often obscure meaningful temporal interactions.

Once the common factors are extracted, FNETS focuses on estimating sparse Granger-causal networks from the idiosyncratic components. This approach allows for a more accurate identification of time series dependencies while mitigating the confounding effects of pervasive factors. The network estimation relies on regularization techniques to manage high-dimensionality and enforce sparsity, making the model scalable even in large datasets.

From a theoretical perspective, FNETS provides rigorous consistency guarantees under assumptions about factor strength, sparsity, and the structure of network connections. These properties make it a powerful tool for applications requiring disentangling large-scale dependencies, such as systemic risk modeling in finance, macroeconomic forecasting, and network analysis in complex systems. Furthermore, by incorporating the estimated network structure into the forecasting framework, FNETS enhances predictive accuracy beyond traditional factor models, offering a more refined understanding of dynamic interdependencies in high-dimensional data environments.

Barigozzi et al. (2024) model a second-order stationary p-variate process $\boldsymbol{X}_t = (X_{1t}, \ldots, X_{pt})$ as a decomposition of two latent components. The model can be described as follows:

$$\boldsymbol{X}_t = \boldsymbol{\chi}_t + \boldsymbol{\xi}_t, \tag{12}$$

$$\boldsymbol{\chi}_t = \mathscr{B}(L)\boldsymbol{u}_t = \sum_{l=0}^{\infty} \boldsymbol{B}_l \boldsymbol{u}_{t-l} \quad \text{with} \quad \boldsymbol{u}_t = (u_{1t}, \ldots, u_{qt})^T, \tag{13}$$

$$\mathscr{A}(L)\xi_t = \xi_t - \sum_{l=1}^{d} A_l \xi_{t-l} = \Gamma^{1/2}\varepsilon_t \quad \text{with} \quad \boldsymbol{\varepsilon}_t = (\varepsilon_{1t}, \ldots, \varepsilon_{pt})^T \tag{14}$$

where $\boldsymbol{\chi}_t = (\chi_{1t}, \ldots, \chi_{qt})$ denotes a factor-driven common component and, $\boldsymbol{\xi}_t = (\xi_{1t}, \ldots, \xi_{pt})$ denotes an idiosyncratic component. The latent vector $\boldsymbol{u}_t$, present in Equation (13), denotes the common factors (common shocks) among the variables and, is assumed to satisfy $E[\boldsymbol{u}_t] = \boldsymbol{0}$ and $Cov[\boldsymbol{u}_t] = \boldsymbol{I}_q$. For each variable i, χ_{it} is computed using the Generalized Dynamic Factor Model (GDFM) formulation (Forni et al., 2000; Forni and Lippi, 2001), which applies square summable one-sided filters $\mathscr{B}_{ij}(L) = \sum_{l=0}^{\infty} B_{l,ij} L^l$, where $\boldsymbol{B}_l = [B_{l,ij}, 1 \leqslant i \leqslant p, 1 \leqslant j \leqslant q] \in \mathbb{R}^{p \times q}$.

On the other hand, Barigozzi et al. (2024) assumes that the idiosyncratic component in Equation (14) follows a VAR process of order d, with innovations denoted as $\Gamma^{1/2}\varepsilon_t$, where it is assumed that $E[\boldsymbol{\varepsilon}_t] = \mathbf{0}$ and $Cov[\boldsymbol{\varepsilon}_t] = \boldsymbol{I}_p$ and $\Gamma^{1/2}$ is a representation of a symmetric square root matrix for some positive definite matrix $\Gamma \in \mathbb{R}^{p \times p}$. Barigozzi et al. (2024) assume that ξ_t is causal and rewrite Equation (14) as a Wold representation as follows:

$$\xi_t = \mathscr{D}(L)\boldsymbol{\Gamma}^{1/2}\varepsilon_t = \sum_{l=0}^{\infty} D_l \boldsymbol{\Gamma}^{1/2}\varepsilon_{t-l} \quad \text{with} \quad \mathscr{D}(L) = \mathscr{A}^{-1}(L), \tag{15}$$

where the idiosyncratic shocks $\boldsymbol{\Gamma}^{1/2}\varepsilon_t$ are loaded for each ξ_{it} through square summable one-sided filters $\mathscr{D}_{ik}(L) = \sum_{l=0}^{\infty} D_{l,ik} L^l$, where $\boldsymbol{D}_l = [D_{l,ik}, 1 \leqslant i,k \leqslant p]$. As Barigozzi et al. (2024) highlights, it is acceptable to assume that the dependence structure left in the idiosyncratic component $\boldsymbol{\xi}_t$ is weak, once the dominant cross-sectional dependence in the data, both lagged and contemporaneous, is captured by common factors in Equation (13), therefore, the VAR structure for the idiosyncratic component is sufficiently sparse.

Since Equations (13) and (14) represent, respectively, the estimation of $\boldsymbol{\chi}_t$ and $\boldsymbol{\xi}_t$, which are latent variables, some assumptions are made by Barigozzi et al. (2024) in order to guarantee (asymptotic) identifiability. These assumptions are made in the frequency domain and are described in the Appendix A.

Before we continue, let us define some notations following Barigozzi et al. (2024). The spectral density matrices of $\boldsymbol{X}_t$, $\boldsymbol{\chi}_t$ and $\boldsymbol{\xi}_t$ at frequency $\omega \in [-\pi, \pi]$ are, respectively, denoted by $\boldsymbol{\Sigma}_x(\omega)$, $\boldsymbol{\Sigma}_\chi(\omega)$ and $\boldsymbol{\Sigma}_\xi(\omega)$. Meanwhile, the dynamics eigenvalues, which are real-valued and in decreasing order, for $\boldsymbol{X}_t$, $\boldsymbol{\chi}_t$ and $\boldsymbol{\xi}_t$ are, respectively, denoted by $\mu_{x,j}(\omega)$, $\mu_{\chi,j}(\omega)$ and $\mu_{\xi,j}(\omega)$.

Using the latent VAR formulation of the idiosyncratic component, presented by Equation (14), and denoting the set of vertices representing the p time series as $\mathscr{V} = 1, \ldots, p$, three different network structures can be analyzed:

1. The first is the Granger causal linkages. In this first network representation, the transition matrices $\boldsymbol{A}_l = [A_{l,ii'}, 1 \leqslant ii' \leqslant p]$ allow the measurement of the directed network $\mathscr{N}^{\mathscr{G}} = (\mathscr{V}, \mathscr{E}^G)$, where

$$\mathscr{E}^G = \{(i,i') \in \mathscr{V} \times \mathscr{V} : A_{l,i,i'} \neq 0 \quad \text{for some} \quad 1 \leqslant l \leqslant d\}$$

represent the set of edges. In this sense, the existence of an edge $(i,i^{'}) \in \mathscr{E}^G$ indicates that the idiosyncratic component of the variable $i^{'}$, in period $t-l$, $\xi_{i^{'},t-l}$ Granger causes the idiosyncratic component of variable i, in period t, $\xi_{i,t}$, for some lag $1 \leqslant l \leqslant d$.

2. The second network representation, $\mathscr{N}^C = (\mathscr{V}, \mathscr{E}^C)$, contains undirected edges and represents the contemporaneous dependence present in VAR innovations $\boldsymbol{\Gamma}^{1/2}\boldsymbol{\varepsilon}_t$. An edge $(i,i^{'})$ is included in $\mathscr{E}^C$ if and only if the partial correlation between the elements i and $i^{'}$ of the innovations $\boldsymbol{\Gamma}^{1/2}\boldsymbol{\varepsilon}_t$ is nonzero. Denoting $\boldsymbol{\Gamma}^{-1} = \Delta = [\delta_{i,i^{'}}, 1 \leqslant i,i^{'} \leqslant p]$, Barigozzi et al. (2024) point out that the set of edges is denoted as follows:

$$\mathscr{E}^C = \left\{ (i,i^{'}) \in \mathscr{V} \times \mathscr{V} : i \neq i^{'} \quad \text{and} \quad -\frac{\delta_{i,i^{'}}}{\sqrt{\delta_{i,i} \cdot \delta_{i^{'},i^{'}}}} \neq 0 \right\}.$$

3. The last structure, as indicated by Barigozzi et al. (2024), uses the long-run partial correlations of $\boldsymbol{\xi}_t$ and is able to summarize the lead-lag and contemporaneous relations in a single undirected network. This network can be denoted as $\mathscr{N}^L = (\mathscr{V}, \mathscr{E}^L)$ and the long-run partial covariance matrix of $\boldsymbol{\xi}_t$ can be represented as $\boldsymbol{\Omega} = [\omega_{ii^{'}}, 1 \leqslant i,i^{'} \leqslant p]$. Under Equation (14), $\boldsymbol{\Omega}$ can be rewritten as $\boldsymbol{\Omega} = (\boldsymbol{\Sigma}_{\xi}(0))^{-1} = 2\pi\mathscr{A}^T(1)\Delta\mathscr{A}(1)$. In this sense, the edges $\mathscr{N}^L$ of this network structure are:

$$\mathscr{E}^L = \left\{ (i,i^{'}) \in \mathscr{V} \times \mathscr{V} : i \neq i^{'} \quad \text{and} \quad -\frac{\omega_{i,i^{'}}}{\sqrt{\omega_{i,i} \cdot \omega_{i^{'},i^{'}}}} \neq 0 \right\}.$$

Barigozzi et al. (2024) emphasizes that, in general, $\mathscr{E}^L$ has higher values than $\mathscr{E}^G \cup \mathscr{E}^C$.

2.4 Network Estimation via FNETS

In this section, following Barigozzi et al. (2024), we will describe the network estimation process, which has three steps.

2.4.1 Step 1: Factor Adjustment via Dynamic PCA

In order to estimate the autocovariance (ACV) matrix of the latent VAR process $\boldsymbol{\xi}_t$, Barigozzi et al. (2024) proposes to explore the gap between the dynamic eigenvalues of the spectral density of $\boldsymbol{X_t}$, which are denoted by $\mu_{x,j}(\omega)$, attributed to common factors $(j \leqslant q)$ and which are not $(j \geqslant q+1)$. This gap, as pointed out by Barigozzi et al. (2024), can be computed using a Dynamic Principal Component Analysis (DPCA) method (Brillinger, 1964, 1981).

Denoting the ACV matrices for $\boldsymbol{X}_t$, $\boldsymbol{\chi}_t$ and $\boldsymbol{\xi}_t$ as, respectively, $\boldsymbol{\Gamma}_x(l) = E[\boldsymbol{X}_{t-l}\boldsymbol{X}_t^T]$, $\boldsymbol{\Gamma}_\chi(l) = E[\boldsymbol{\chi}_{t-l}\boldsymbol{\chi}_t^T]$ and $\boldsymbol{\Gamma}_\xi(l) = E[\boldsymbol{\xi}_{t-l}\boldsymbol{\xi}_t^T]$, for $l \geqslant 0$. Also, for $l \leqslant -1$, the ACV matrices can be rewritten as $\boldsymbol{\Gamma}_x(l) = \boldsymbol{\Gamma}_x^T(-l)$, $\boldsymbol{\Gamma}_\chi(l) = \boldsymbol{\Gamma}_\chi^T(-l)$ and $\boldsymbol{\Gamma}_\xi(l) = \boldsymbol{\Gamma}_\xi^T(-l)$. Therefore, Barigozzi et al. (2024) highlights that the spectral density matrix and the ACV matrix for $\boldsymbol{X}_t$, $\boldsymbol{\Sigma}_x(\omega)$ and $\boldsymbol{\Gamma}_x(l)$, satisfy the following equation:

$$\boldsymbol{\Sigma}_x(\omega) = \frac{1}{2\pi}\sum_{l=-\infty}^{\infty} \boldsymbol{\Gamma}_x(l)\exp(-il\omega), \quad \text{for all} \quad \omega \in [-\pi,\pi], \tag{16}$$

and, therefore, $\boldsymbol{\Sigma}_x(\omega)$ can be estimated as

$$\hat{\boldsymbol{\Sigma}}_x(\omega) = \frac{1}{2\pi}\sum_{l=-m}^{m} K\left(\frac{l}{m}\right)\hat{\boldsymbol{\Gamma}}_x(l)\exp(-il\omega), \tag{17}$$

where $\hat{\boldsymbol{\Gamma}}_x(l) = n^{-1}\sum_{t=l+1}^{n}\boldsymbol{X}_{t-l}\boldsymbol{X}_t^T$ represents the sample ACV, for $l \geqslant 0$, and $\hat{\boldsymbol{\Gamma}}_x(l) = \hat{\boldsymbol{\Gamma}}_x(-l)^T$, for $l < 0$. For guarantee the positive semi-definiteness of $\hat{\boldsymbol{\Sigma}}_x(\omega)$, Barigozzi et al. (2024) assume $K(\cdot)$ as a Bartlett kernel, with kernel bandwidth given by $m = [n^\beta]$, for $\beta \in (0,1)$.

As in Barigozzi et al. (2024), $\hat{\boldsymbol{\Sigma}}_x(\omega)$ is measured at $2m+1$ Fourier frequencies $\omega_k = 2\pi k/(2m+1)$, for $0 \leqslant k \leqslant m$ and $\omega_k = -\omega_{|k|}$, for $-m \leqslant k \leqslant -1$. Meanwhile, the spectral density matrix $\boldsymbol{\Sigma}_\chi(\omega_k)$ can be computed using only the contribution of the q largest eigenvalues and eigenvectors as follows:

$$\hat{\boldsymbol{\Sigma}}_\chi(\omega_k) = \sum_{j=1}^{q} \hat{\mu}_{x,j}(\omega_k)\hat{\boldsymbol{e}}_{x,j}(\omega_k)(\hat{\boldsymbol{e}}_{x,j}(\omega_k))^*, \tag{18}$$

where $(\hat{\boldsymbol{e}}_{x,j}(\omega_k))^*$ denote the transposed complex conjugate matrix of $\hat{\boldsymbol{e}}_{x,j}(\omega_k)$ and the j leading eigenvalues and j associated (normalized) eigenvectors of $\hat{\boldsymbol{\Sigma}}_x(\omega)$ are denoted, respectively, by $\hat{\mu}_{x,j}(\omega_k)$ and $\hat{\boldsymbol{e}}_{x,j}(\omega_k)$. In this sense, Barigozzi et al. (2024) pointed out that an estimator for the ACV matrix for $\boldsymbol{\chi}_t$, for a given lag $l \in \mathbb{N}$, can be constructed as the inverse of Fourier transform as follows:

$$\hat{\mathbf{\Gamma}}_{\chi}(l) = 2\pi(2m+1)^{-1}\sum_{k=-m}^{m}\hat{\mathbf{\Sigma}}_{\chi}(\omega_k)\exp(il\omega_k). \tag{19}$$

Therefore, by Assumption 4 (*3*), the ACV matrices of $\boldsymbol{\xi}_t$ can be computed as follows:

$$\hat{\mathbf{\Gamma}}_{\xi}(l) = \hat{\mathbf{\Gamma}}_{x}(l) - \hat{\mathbf{\Gamma}}_{\chi}(l). \tag{20}$$

2.4.2 Step 2: Estimation of VAR Parameters and $\mathscr{N}^G$

In the second step, the VAR parameters of Equation (14) are estimated as $\boldsymbol{\beta} = [\boldsymbol{A}_l, 1 \leqslant l \leqslant d]^T \in \mathbb{R}^{(pd)\times p}$. Barigozzi et al. (2024) estimates these parameters using the following Yule-Walker (YW) representation:

$$\boldsymbol{\beta} = \mathbb{G}^{-1}g, \tag{21}$$

where

$$\mathbb{G} = \begin{bmatrix} \mathbf{\Gamma}_{\xi}(0) & \mathbf{\Gamma}_{\xi}(-1) & \cdots & \mathbf{\Gamma}_{\xi}(-d+1) \\ \vdots & \vdots & \ddots & \vdots \\ \mathbf{\Gamma}_{\xi}(d-1) & \mathbf{\Gamma}_{\xi}(d-2) & \cdots & \mathbf{\Gamma}_{\xi}(0) \end{bmatrix} \quad \text{and}$$

$$g = \begin{bmatrix} \mathbf{\Gamma}_{\xi}(1) \\ \vdots \\ \mathbf{\Gamma}_{\xi}(d) \end{bmatrix},$$

where, by Assumption 3 (*3*), $\mathbb{G}$ always has an inverse representation. Therefore, substituting $\mathbf{\Gamma}_{\xi}(l)$ for those obtain in first step, $\hat{\mathbf{\Gamma}}_{\xi}(l)$, in $\mathbb{G}$ and g, the $\boldsymbol{\beta}$ can be computed through an l_1-penalised M-estimation as follows:

$$\hat{\boldsymbol{\beta}} = \arg\min_{M\in\mathbb{R}^{(pd)\times p}} \boldsymbol{tr}(\boldsymbol{M}^T\hat{\mathbb{G}}\boldsymbol{M} - 2\boldsymbol{M}^T\hat{g}) + \lambda|\boldsymbol{M}|_1, \tag{22}$$

where λ represents the tuning parameters, which is strictly positive. Since the matrix $\hat{\mathbb{G}}$ is guaranteed to be positive semi-definite, according to Barigozzi et al. (2024), the problem (22)* is convex and has a global minimum solution.

*Barigozzi et al. (2024) point to the similarities with the Lasso estimator, however, in the problem (22), the estimation of the parameters of the latent VAR process, $\boldsymbol{\xi}_t$, occurs only by means of second-order moments.

Therefore, once we have $\boldsymbol{\beta}$, the set of edges $\mathscr{N}^G$ can be estimated using $\hat{\boldsymbol{\beta}}(t) = [\hat{\beta}_{ij} \cdot \mathbb{I}_{\{|\hat{\beta}_{ij}|>t\}}]$, where $\mathbb{I}_{\{|\hat{\beta}_{ij}|>t\}}$ denote some threshold $t > 0$.

2.4.3 Step 3: Estimation of $\mathscr{N}^C$ and $\mathscr{N}^L$

In the final estimation step, the set of edges of $\mathscr{N}^C$ and $\mathscr{N}^L$ is measured. In order to compute Δ and Ω, which are necessary to measure those two sets, Barigozzi et al. (2024) proposes to extend, to a time series data set, the estimation process of the precision matrix of independent data proposed by Cai et al. (2011). The method proposed by Barigozzi et al. (2024), which estimates $\Delta = \boldsymbol{\Gamma}^{-1}$ via constrained l_1-minimization, can be described as follows:

$$\check{\Delta} = \arg \min_{\boldsymbol{M} \in \mathbb{R}^{p \times p}} |\boldsymbol{M}|_1 \tag{23}$$

$$\text{s.t.} \quad |\hat{\boldsymbol{\Gamma}} \boldsymbol{M} - \boldsymbol{I}|_\infty \leqslant \eta, \tag{24}$$

where η represents the tuning parameters, which is strictly positive, and $\hat{\boldsymbol{\Gamma}} = \hat{\boldsymbol{\Gamma}}_\xi(0) - \hat{\boldsymbol{\beta}}^T \hat{g}$. However, as the solution in $\check{\Delta}$ does not guarantee symmetry, a symmetrization step is required:

$$\hat{\boldsymbol{\Delta}} = [\hat{\delta}_{ii'}, 1 \leqslant i, i' \leqslant p] \quad \text{with}$$
$$\hat{\delta}_{ii'} = \check{\delta}_{ii'} \cdot \mathbb{I}_{\{|\check{\delta}_{ii'}| \leqslant |\check{\delta}_{i'i}|\}} + \check{\delta}_{i'i} \cdot \mathbb{I}_{\{|\check{\delta}_{i'i}| < |\check{\delta}_{ii'}|\}}.$$

In this sense, the set of edges $\mathscr{N}^C$ can be estimated using $\hat{\boldsymbol{\Delta}}(t_\delta) = [\hat{\delta}_{ii'} \cdot \mathbb{I}_{\{|\hat{\delta}_{ii'}|>t_\delta\}}, 1 \leqslant i, i' \leqslant p]$, for some threshold $t_\delta > 0$.

The last set of edges, $\mathscr{N}^L$, can be computed substituting the estimates of $\mathscr{A}(1)$ and Δ in $\boldsymbol{\Omega} = 2\pi(\mathscr{A}(1))^T \boldsymbol{\Delta} \mathscr{A}(1)$, thus, as $\hat{\boldsymbol{\Omega}} = 2\pi(\hat{\mathscr{A}}(1))^T \hat{\boldsymbol{\Delta}} \hat{\mathscr{A}}(1)$, where $\hat{\mathscr{A}}(1) = \boldsymbol{I} - \sum_{l=1}^d \hat{\mathscr{A}}_l(t)$. Therefore, the set of edges for $\mathscr{N}^L$ can be estimated using $\hat{\boldsymbol{\Omega}} = [\hat{\omega}_{ii'} \cdot \mathbb{I}_{\{|\hat{\omega}_{ii'}|>t_\omega\}}, 1 \leqslant i, i' \leqslant p]$ with some threshold $t_\omega > 0$.

To enhance methodological transparency and reproducibility, we summarize our integrated FNETS-SV framework through a structured pseudo-algorithm (Box 1). This computational blueprint systematically outlines the four-stage estimation process: (1) univariate stochastic volatility (SV) estimation via Integrated Nested Laplace Approximations (INLA), (2) dynamic factor adjustment through spectral decomposition, (3) l_1-regularized VAR parameter estimation via Yule-Walker equations, and (4) network construction from Granger-causal, contemporaneous, and long-run dependencies.

Algorithm 1 FNETS-SV Estimation Core Process

Input:
Price data $\{P_{i,t}\}$ for p assets ($i = 1,\ldots,p$) over $t = 1,\ldots,T$
Output:
Volatility networks $\mathscr{E}^G$, $\mathscr{E}^C$, $\mathscr{E}^L$
procedure MAIN
// Stage 1: Univariate Stochastic Volatility Estimation
for each asset $i \in \{1,\ldots,p\}$ **do**
Compute log-returns: $y_{i,t} = \log(P_{i,t}/P_{i,t-1})$
Estimate SV model via INLA:
$y_t = \exp\{h_t/2\}\varepsilon_t, \quad \varepsilon_t \sim \text{i.i.d. } \mathscr{N}(0,1)$
$h_t = \mu + \phi(h_{t-1} - \mu) + \eta_t, \quad \eta_t \sim \text{i.i.d. } \mathscr{N}(0,\sigma_\eta^2)$
end for
Set $X_{i,t} = \log(\sigma_{i,t})$ to ensure positivity of the volatility estimate using the FNETS method.
// Stage 2: Factor Adjustment
Construct spectral density matrix for $\mathbf{X}_t$, $\hat{\Sigma}_x(\omega)$, using Bartlett kernel:
$\hat{\mathbf{\Sigma}}_x(\omega) = \frac{1}{2\pi}\sum_{l=-m}^{m} K\left(\frac{l}{m}\right)\hat{\mathbf{\Gamma}}_x(l)\exp(-il\omega)$
Apply spectral decomposition to decompose $\hat{\mathbf{\Sigma}}_x(\omega)$ into eigenvectors and eigenvalues.
Compute the spectral density matrix for $\boldsymbol{\chi}_t$ using only the contribution of the q largest eigenvalues and eigenvectors:
$\hat{\mathbf{\Sigma}}_\chi(\omega_k) = \sum_{j=1}^{q}\hat{\mu}_{x,j}(\omega_k)\hat{\boldsymbol{e}}_{x,j}(\omega_k)(\hat{\boldsymbol{e}}_{x,j}(\omega_k))^*$
Compute the ACV matrix for $\boldsymbol{\chi}_t$, for a given lag $l \in \mathbb{N}$, as:
$\hat{\mathbf{\Gamma}}_\chi(l) = 2\pi(2m+1)^{-1}\sum_{k=-m}^{m}\hat{\mathbf{\Sigma}}_\chi(\omega_k)\exp(il\omega_k)$
Compute $\mathbf{\Gamma}_\xi(l)$:
$\hat{\Gamma}_\xi(l) = \hat{\Gamma}_x(l) - \hat{\Gamma}_\chi(l)$
// Stage 3: Sparse VAR Estimation
Solve regularized Yule-Walker equations:
$\hat{\boldsymbol{\beta}} = \arg\min_{M \in \mathbb{R}^{(pd)\times p}} \boldsymbol{tr}(\boldsymbol{M}^T\hat{\mathbb{G}}\boldsymbol{M} - 2\boldsymbol{M}^T\hat{g}) + \lambda|\boldsymbol{M}|_1$
// Stage 4: Network Construction
Granger network $\mathscr{E}^G$:
$\hat{\boldsymbol{\beta}}(t) = [\hat{\beta}_{ij}\cdot\mathbb{I}_{\{|\hat{\beta}_{ij}|>t\}}]$, where $\mathbb{I}_{\{|\hat{\beta}_{ij}|>t\}}$ denotes some threshold $t > 0$
$\mathscr{E}^G = \{(i,i') \in \mathscr{V}\times\mathscr{V} : A_{l,i,i'} \neq 0 \quad \text{for some} \quad 1 \leqslant l \leqslant d\}$
Contemporaneous network $\mathscr{E}^C$:
$\hat{\mathbf{\Delta}}(t_\delta) = [\hat{\delta}_{ii'}\cdot\mathbb{I}_{\{|\hat{\delta}_{ii'}|>t_\delta\}}, 1 \leqslant i,i' \leqslant p]$, for some threshold $t_\delta > 0$
$\mathscr{E}^C = \{(i,i') \in \mathscr{V}\times\mathscr{V} : i \neq i' \quad \text{and} \quad -\delta_{i,i'}/\sqrt{\delta_{i,i}\cdot\delta_{i',i'}} \neq 0\}$
Long-run network $\mathscr{E}^L$:
$\hat{\mathbf{\Omega}} = [\hat{\omega}_{ii'}\cdot\mathbb{I}_{\{|\hat{\omega}_{ii'}|>t_\omega\}}, 1 \leqslant i,i' \leqslant p]$ with some threshold $t_\omega > 0$
$\mathscr{E}^L = \{(i,i') \in \mathscr{V}\times\mathscr{V} : i \neq i' \quad \text{and} \quad -\omega_{i,i'}/\sqrt{\omega_{i,i}\cdot\omega_{i',i'}} \neq 0\}$
end procedure

2.5 Data

The data used in this study consists of 82 stocks from the theoretical Ibovespa Index portfolio, valid for the period from January to April 2025. The analyzed period spans from January 3, 2022, to January 28, 2025. Not all companies listed in the theoretical Ibovespa portfolio were included in the analysis, as some stocks had a limited number of trading days during this timeframe. Consequently, only stocks with continuous market activity throughout the post-pandemic period (2022–2025) were considered.

To ensure positive volatility values, we define $X_{i,t} = \log(\sigma_{i,t})$, where i represents the asset in period t.

Table 1 presents the descriptive statistics for the volatility estimates obtained from a Stochastic Volatility model estimated using Integrated Nested Laplace Approximation (INLA). The assets are ordered from highest to lowest volatility based on the median. Notably, MGLU3 (median = 0.045) and CVCB3 (median = 0.042) exhibit the highest volatility, while EGIE3 (median = 0.010) and TAEE11 (median = 0.009) display the lowest values. Additionally, Figure 1 shows the sample correlation matrix heatmap for the SV volatility. Most correlation values outside the main diagonal are positive and fall within the range of 0.2 to 0.6.

3. Empirical Results

We present the results of our analysis using heatmaps, which provide an intuitive and concise way to summarize the patterns observed across a large number of assets. This section discusses the heatmaps that capture different aspects of the interdependencies within the volatility network of the Brazilian stock market. By jointly examining the Granger Causal, Partial Correlation (PC), and Long-Run Partial Correlation (LRPC) heatmaps, we gain a comprehensive understanding of the dynamic, instantaneous, and persistent relationships governing this high-dimensional time series.

Figure 2 presents the Granger Causal heatmap, constructed using Univariate Stochastic Volatility (SV) models as the volatility measurement method. This heatmap illustrates directed temporal dependencies inferred from the sparse vector autoregressive (VAR) coefficients, highlighting lead-lag relationships among variables. Each cell represents the strength of Granger causality from one asset to another, controlling for common factors.

As expected, the diagonal elements exhibit high values, reflecting the strong autocorrelation within each time series. In contrast, the off-diagonal elements—particularly the darker ones—indicate significant causal links between different assets, suggesting that the past volatility of one asset con-

Table 1
Descriptive Statistics

	Mean	Std.	Skew.	Kurt.	Min.	5% Quantile	Median	95% Quantile	Max.
MGLU3	0.045	0.008	0.452	3.379	0.030	0.033	0.045	0.058	0.070
CVCB3	0.042	0.010	0.500	3.743	0.020	0.028	0.042	0.060	0.081
AZUL4	0.038	0.009	3.601	24.221	0.029	0.030	0.035	0.053	0.124
LWSA3	0.037	0.008	0.545	2.289	0.024	0.026	0.035	0.053	0.058
PETZ3	0.035	0.006	2.771	18.749	0.026	0.028	0.033	0.045	0.094
HAPV3	0.035	0.014	2.943	15.193	0.019	0.021	0.032	0.054	0.124
YDUQ3	0.032	0.006	2.488	12.578	0.025	0.026	0.030	0.044	0.083
MRVE3	0.030	0.005	2.140	9.584	0.024	0.025	0.028	0.039	0.059
COGN3	0.030	0.004	2.377	11.652	0.025	0.025	0.028	0.038	0.064
LREN3	0.028	0.002	0.788	3.046	0.024	0.025	0.027	0.033	0.035
NTCO3	0.029	0.008	0.781	3.365	0.015	0.019	0.027	0.045	0.062
IRBR3	0.030	0.011	2.016	9.508	0.015	0.018	0.027	0.053	0.103
PCAR3	0.030	0.014	9.264	153.948	0.016	0.019	0.027	0.048	0.293
BRFS3	0.027	0.008	1.178	4.361	0.016	0.018	0.026	0.043	0.059
CRFB3	0.026	0.005	0.805	4.297	0.015	0.019	0.026	0.035	0.045
VAMO3	0.027	0.005	2.208	8.986	0.023	0.023	0.025	0.038	0.057
CSNA3	0.026	0.007	0.321	2.271	0.013	0.015	0.025	0.038	0.049
RAIZ4	0.025	0.005	0.068	1.602	0.017	0.018	0.024	0.033	0.034
ASAI3	0.025	0.006	0.683	2.927	0.016	0.017	0.024	0.036	0.043
MRFG3	0.025	0.004	1.898	8.012	0.020	0.021	0.024	0.033	0.048
RECV3	0.024	0.005	1.845	12.543	0.016	0.018	0.023	0.033	0.068
BRKM5	0.024	0.006	3.148	20.747	0.017	0.018	0.023	0.034	0.076
VIVA3	0.023	0.004	0.346	3.151	0.015	0.017	0.023	0.030	0.041
AZZA3	0.023	0.005	0.350	2.600	0.015	0.016	0.023	0.032	0.038
RDOR3	0.024	0.005	0.459	2.074	0.015	0.017	0.023	0.034	0.035
CMIN3	0.023	0.004	1.563	6.039	0.018	0.019	0.022	0.031	0.040
CYRE3	0.023	0.004	1.484	6.223	0.017	0.018	0.022	0.031	0.047
STBP3	0.021	0.008	-0.237	3.667	0.002	0.004	0.022	0.036	0.051
SMTO3	0.022	0.004	1.179	4.262	0.016	0.017	0.022	0.032	0.037
PRIO3	0.024	0.005	0.560	1.994	0.017	0.018	0.022	0.033	0.035
B3SA3	0.022	0.005	0.812	2.876	0.016	0.017	0.021	0.032	0.035
VBBR3	0.021	0.003	0.055	2.057	0.016	0.016	0.021	0.026	0.027
USIM5	0.022	0.007	1.571	11.568	0.008	0.012	0.021	0.033	0.080
BPAC11	0.021	0.005	0.501	2.222	0.014	0.015	0.020	0.031	0.033
RENT3	0.021	0.005	1.785	9.404	0.014	0.016	0.020	0.030	0.053
PETR4	0.020	0.006	0.366	2.753	0.009	0.011	0.020	0.031	0.034
BEEF3	0.022	0.005	3.198	22.034	0.016	0.017	0.020	0.031	0.072
CSAN3	0.020	0.004	1.042	4.135	0.014	0.016	0.020	0.028	0.034
UGPA3	0.021	0.005	0.383	2.115	0.012	0.014	0.020	0.030	0.032
POMO4	0.021	0.004	2.584	15.446	0.016	0.017	0.020	0.030	0.060
EMBR3	0.021	0.005	2.577	14.486	0.015	0.016	0.019	0.030	0.065
TOTS3	0.020	0.005	1.132	4.715	0.012	0.014	0.019	0.030	0.047
FLRY3	0.018	0.005	0.128	1.667	0.011	0.012	0.019	0.026	0.031
IGTI11	0.019	0.005	0.612	2.390	0.012	0.013	0.018	0.029	0.034
ENEV3	0.019	0.004	0.517	3.088	0.012	0.013	0.018	0.026	0.032
ELET3	0.018	0.003	0.450	2.130	0.014	0.015	0.018	0.024	0.025
RAIL3	0.018	0.004	0.848	3.066	0.011	0.014	0.017	0.026	0.028
MULT3	0.018	0.004	0.841	3.477	0.011	0.012	0.017	0.027	0.031
VALE3	0.018	0.005	0.462	2.606	0.010	0.011	0.017	0.026	0.031
JBSS3	0.018	0.003	1.778	8.809	0.013	0.014	0.017	0.024	0.040
BRAP4	0.017	0.003	0.073	2.083	0.011	0.012	0.017	0.022	0.025
HYPE3	0.017	0.003	1.906	8.955	0.013	0.014	0.017	0.023	0.037
SBSP3	0.017	0.004	1.546	8.875	0.011	0.011	0.017	0.023	0.041
ELET6	0.017	0.003	0.103	2.033	0.011	0.012	0.017	0.022	0.023
GGBR4	0.017	0.004	1.809	7.297	0.013	0.014	0.016	0.025	0.038
PETR3	0.018	0.004	2.716	13.192	0.014	0.014	0.016	0.026	0.047
ENGI11	0.016	0.003	0.289	2.392	0.012	0.012	0.016	0.021	0.023
RADL3	0.017	0.003	0.520	2.278	0.011	0.013	0.016	0.022	0.024
GOAU4	0.016	0.003	1.996	8.622	0.013	0.013	0.015	0.023	0.037
CCRO3	0.016	0.004	0.703	2.987	0.010	0.011	0.015	0.023	0.029
CMIG4	0.016	0.004	1.519	7.198	0.009	0.011	0.015	0.023	0.040
SLCE3	0.016	0.005	1.019	4.196	0.008	0.009	0.015	0.025	0.038
SANB11	0.015	0.002	0.837	4.398	0.010	0.011	0.014	0.019	0.026
SUZB3	0.015	0.003	3.652	28.654	0.012	0.013	0.014	0.021	0.047
CXSE3	0.015	0.004	0.602	2.640	0.009	0.009	0.014	0.022	0.027
ITUB4	0.014	0.003	0.436	2.064	0.009	0.010	0.014	0.019	0.020
WEGE3	0.015	0.005	1.582	6.542	0.008	0.010	0.014	0.025	0.042
KLBN11	0.014	0.002	0.397	1.851	0.011	0.011	0.014	0.019	0.020
BBAS3	0.015	0.005	0.935	3.428	0.009	0.009	0.014	0.024	0.029
CPLE6	0.015	0.004	3.207	18.955	0.010	0.011	0.014	0.020	0.047
TIMS3	0.014	0.002	2.241	9.641	0.012	0.012	0.013	0.017	0.025
BBDC4	0.014	0.005	5.250	51.944	0.010	0.010	0.013	0.021	0.068
EQTL3	0.013	0.003	3.151	20.052	0.010	0.011	0.013	0.019	0.040
CPFE3	0.013	0.004	0.932	3.408	0.007	0.008	0.012	0.021	0.027
ITSA4	0.012	0.002	1.117	6.184	0.009	0.010	0.012	0.016	0.025
PSSA3	0.013	0.004	2.081	9.137	0.009	0.009	0.012	0.020	0.035
BBDC3	0.013	0.004	5.482	55.087	0.010	0.010	0.012	0.019	0.061
ABEV3	0.012	0.003	1.122	4.869	0.007	0.008	0.012	0.018	0.025
VIVT3	0.012	0.002	1.891	7.588	0.009	0.010	0.011	0.017	0.025
BBSE3	0.011	0.003	1.439	5.914	0.007	0.008	0.010	0.016	0.023
EGIE3	0.011	0.002	1.031	4.222	0.007	0.008	0.010	0.014	0.019
TAEE11	0.009	0.002	0.943	4.169	0.005	0.006	0.009	0.013	0.020

Note: This table presents the mean, standard deviation (Std.), skewness (Skew.), kurtosis (Kurt.), minimum (Min.), 5% Quantile (lower tail bound), Median (central tendency measure), 95% Quantile (upper tail bound) and maximum (Max.) for 771 observations of volatility estimates obtained from a Stochastic Volatility model estimated using Integrated Nested Laplace Approximation (INLA).

Figure 1
Sample Correlation Matrix Heatmap

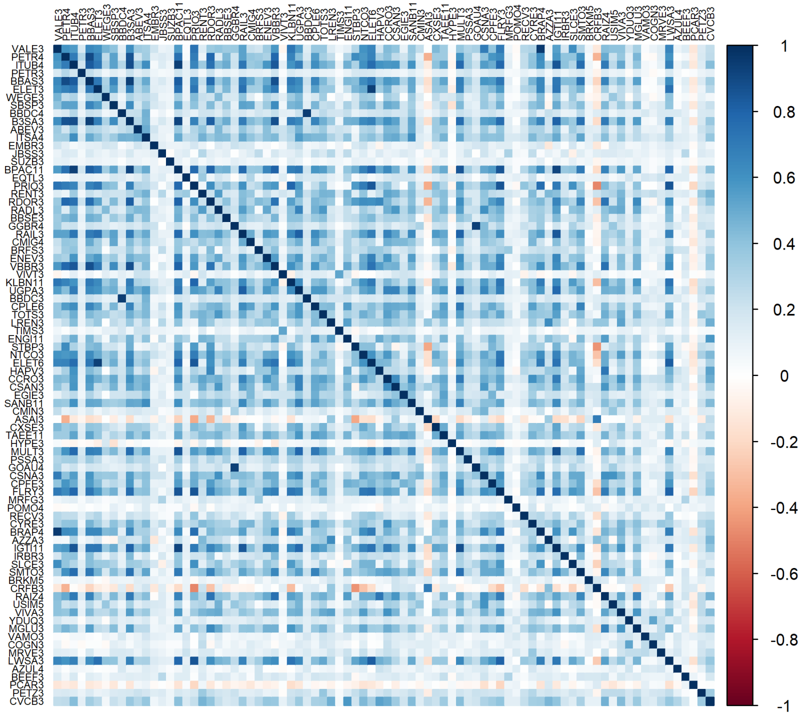

Note: This figure illustrates sample correlation matrix of volatility estimates derived from a Stochastic Volatility model estimated via Integrated Nested Laplace Approximation (INLA), based on 771 observations.

tributes to predicting the volatility of another beyond shared market factors.

Most off-diagonal elements in the Granger Causal network are close to zero, implying that, in general, an asset's volatility is primarily influenced by its own past values. In other words, the volatility of asset i is largely driven by its own lagged volatility. However, certain exceptions emerge, where the lagged volatility of asset j significantly influences asset i, as observed in the case of PETR3's lagged volatility affecting the volatility of PETR4.

Figure 3 presents the Partial Correlation (PC) heatmap, estimated using the FNETS method. This heatmap is derived from the inverse covariance ma-

Figure 2
Granger causal for Univariate SV models

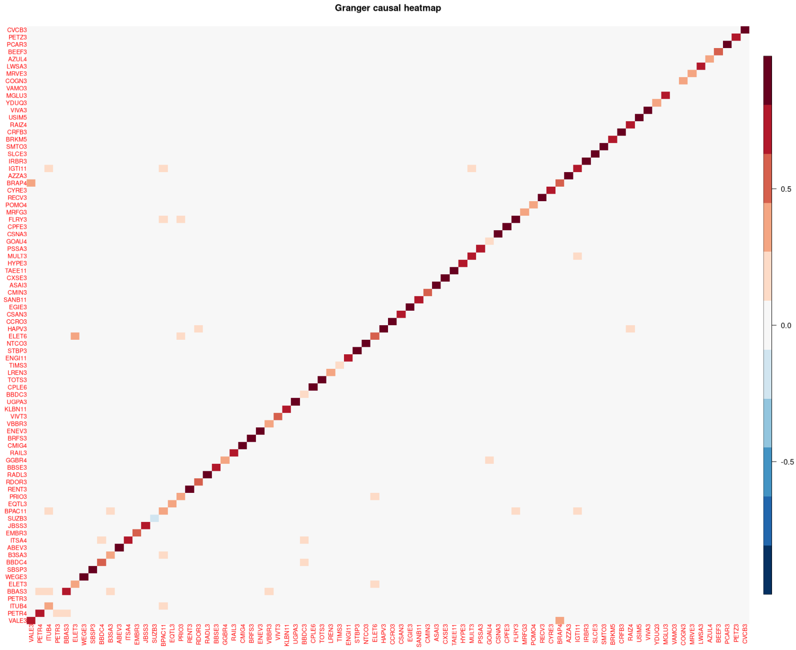

trix of the factor-adjusted residuals and reveals undirected contemporaneous linkages in the volatility network that persist after accounting for common factors.

A notable feature of the PC heatmap is the pronounced sparsity and the predominance of neutral hues (near-white tones) in the upper-right quadrant, which corresponds to assets with minimal weighting in the theoretical Ibovespa (IBOV) portfolio. This pattern suggests weaker direct contemporaneous connections among these assets.

This spatial arrangement aligns with the structural characteristics of the portfolio composition, where peripheral firms exhibit limited pairwise interdependencies. This is reflected in the lower edge density and weaker correlation magnitudes within the factor-adjusted network. These findings highlight the heterogeneous connectivity structure of the volatility network, where an asset's centrality in the portfolio influences its role in systemic interactions.

Figure 4 presents the Long-Run Partial Correlation (LRPC) heatmap, estimated using the FNETS method. This heatmap is derived from the inverse

Figure 3
Partial Correlations (Contemporaneous Dependence) - Univariate SV models

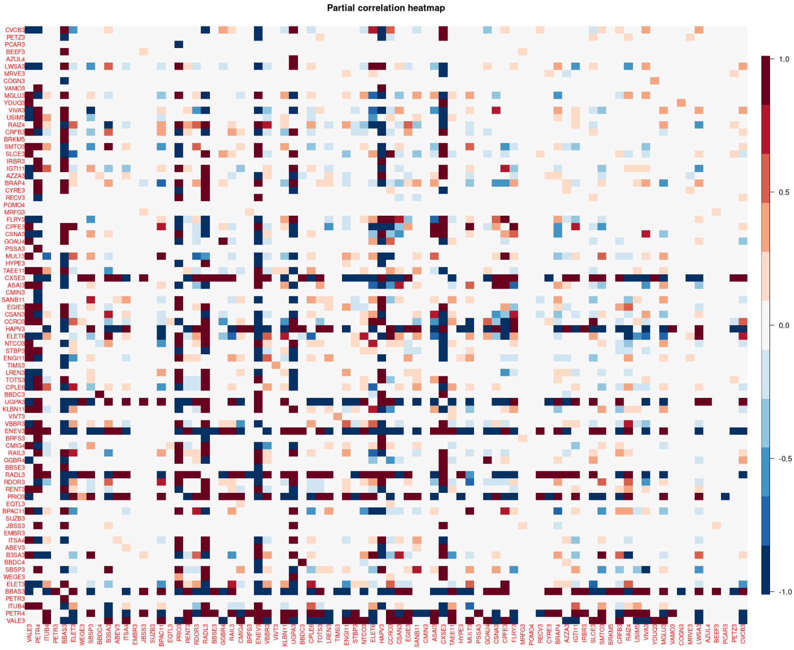

spectral density matrix at frequency zero, capturing both transient and persistent interdependencies to provide a comprehensive view of systemic connectivity.

A striking feature of the LRPC heatmap is the heightened sparsity and predominance of near-zero correlations in the upper-right quadrant, which corresponds to assets with marginal weights in the theoretical Ibovespa (IBOV) portfolio. This pattern closely mirrors the structure observed in the Partial Correlation (PC) heatmap.

The consistency across heatmaps highlights the attenuated direct and long-run linkages among peripheral firms, reinforcing the hypothesis that assets with limited representation in the portfolio tend to exhibit weaker systemic interactions.

4. Robustness

To evaluate the robustness of our estimation approach, we compared the volatility forecasts obtained using the FNETS methodology, based on the

Figure 4
Long-Run Partial Correlations - Univariate SV models

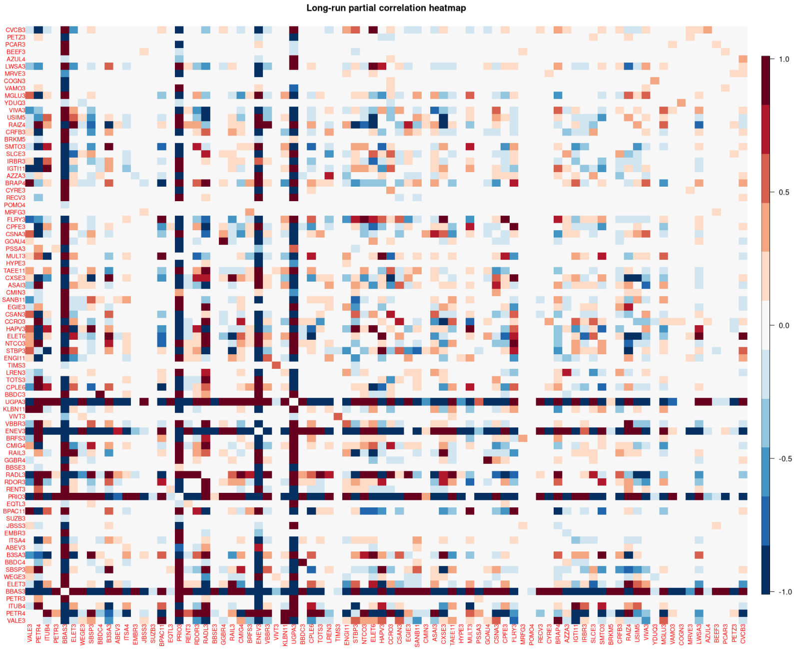

univariate SV model estimated via INLA, with those derived from two alternative volatility measures: the Open-High-Low-Close (OHLC) estimator, introduced by Garman and Klass (1980), and the High-Low (HL) estimator, proposed by Parkinson (1980).

The OHLC measure, in particular, is widely recognized as one of the most commonly used methods for quantifying volatility spillovers (Yilmaz, 2010; Diebold and Yilmaz, 2011, 2012, 2015; Cotter et al., 2023; Korobilis and Yilmaz, 2018; Demirer et al., 2018; Bostanci and Yilmaz, 2020; Demirer et al., 2019). Meanwhile, the HL measure was selected for comparison due to its application in Barigozzi et al. (2024).

We now outline the forecasting procedure as proposed by Barigozzi et al. (2024). The forecast for $\boldsymbol{X}_{n+a}$ given $\boldsymbol{X}_t$, for $t \leqslant n$ and $a \geqslant 1$, is obtained by decomposing the best linear predictors for the common factors, $\boldsymbol{\chi}_{n+a}$, and the idiosyncratic component, $\boldsymbol{\xi}_{n+a}$. Denoting $a \geqslant 0$ as the forecasting horizon, we have

$$\boldsymbol{\chi}_{n+a|n} = \sum_{l=0}^{\infty} \boldsymbol{B}_{l+a} \boldsymbol{u}_{n-l}, \tag{25}$$

where $\boldsymbol{\chi}_{n+a|n}$ represents the best linear predictor of $\boldsymbol{\chi}_{n+a}$ given $\boldsymbol{\chi}_{n-l}$, for $l \geqslant 0$. Without imposing additional restrictions on the estimation of the common factor model (Equation (13)), Barigozzi et al. (2024) indicate that the estimator of $\boldsymbol{\chi}_{n+a|n}$ is given by:

$$\hat{\boldsymbol{\chi}}^{\text{unr}}_{n+a|n} = \sum_{l=0}^{K} \hat{\boldsymbol{B}}_{l+a} \hat{\boldsymbol{u}}_{n-l}, \tag{26}$$

for a certain truncation lag K. According to (Barigozzi et al., 2024), the in-sample estimators of $\boldsymbol{\chi}_t$, for $t \leqslant n$, can be obtained as $\hat{\boldsymbol{\chi}}^{\text{unr}}_{t|n} = \hat{\boldsymbol{\chi}}^{\text{unr}}_{t}$. Regarding the idiosyncratic component forecasts, the best linear predictor of $\boldsymbol{\xi}_{n+a}$ based on $\boldsymbol{X}_t$, for $t \leqslant n$, can be described as follows:

$$\hat{\boldsymbol{\xi}}_{n+a|n} = \sum_{l=1}^{\max(1,a)-1} \hat{\boldsymbol{A}}_l \hat{\boldsymbol{\xi}}_{n+a-l|n} + \sum_{l=\max(1,a)}^{d} \hat{\boldsymbol{A}}_l \hat{\boldsymbol{\xi}}_{n+a-l}, \tag{27}$$

where, according to (Barigozzi et al., 2024), the in-sample estimator for the idiosyncratic component $\boldsymbol{\xi}_t$ is recovered by $\hat{\boldsymbol{\xi}}_t = \boldsymbol{X}_t - \hat{\boldsymbol{\chi}}^{\text{unr}}_t$.

Table 2 reports the error metrics for three types of forecasting models, evaluated using Mean Absolute Error (MAE), Mean Absolute Percentage Error (MAPE), and Mean Squared Error (MSE). These metrics provide a comprehensive assessment of the models' predictive accuracy and robustness.

When analyzing the MAE, it becomes evident that models incorporating stochastic volatility (SV) generally yield lower absolute errors compared to the OHLC and HL models. For instance, in the case of the VALE3 asset, the MAE for the SV model is 4.11455, whereas for the OHLC and HL models, it is 4.61450 and 4.61386, respectively. The MAPE, which measures the relative percentage error, follows a similar trend, with the SV model consistently exhibiting lower percentage errors across most assets compared to the OHLC and HL models.

The MSE, which penalizes larger deviations due to its quadratic nature, further highlights the superior performance of the SV model. For example, for the VALE3 asset, the MSE for the SV model is 16.95744, while for the OHLC

Table 2
Error Metrics

		MAE			MAPE			MSE	
	SV	OHLC	HL	SV	OHLC	HL	SV	OHLC	HL
VALE3	4.11455	4.61450	4.61386	0.98315	0.99962	0.99749	16.95744	21.91202	21.59300
PETR4	3.94472	4.35562	4.35890	0.96523	1.00010	0.99730	15.60184	19.15866	19.20309
ITUB4	4.31359	4.49935	4.52242	0.98924	0.99995	0.99781	18.64222	20.38708	20.60280
PETR3	4.05481	4.31666	4.31899	0.99334	1.00021	0.99797	16.47763	18.79749	18.82948
BBAS3	4.25538	4.57028	4.58640	0.97072	1.00043	0.99104	18.17933	21.36937	22.32752
ELET3	4.03512	4.22254	4.25219	0.98950	1.00009	0.99850	16.29561	17.96249	18.23345
WEGE3	4.28989	4.35494	4.38961	0.99300	0.99896	0.99916	18.42605	19.11578	19.41717
SBSP3	4.10968	4.27128	4.29463	0.98695	1.00007	0.99852	16.90673	18.38387	18.59117
BBDC4	4.26213	4.35078	4.37402	0.98904	1.00044	0.99709	18.22740	19.24505	19.46561
B3SA3	3.86479	4.09250	4.11622	0.98462	0.99997	0.99796	14.96793	16.88339	17.08754
ABEV3	4.47928	4.45198	4.49696	0.99805	1.00004	0.99910	20.08117	19.97169	20.38404
ITSA4	4.41210	4.54260	4.57702	0.99642	1.00017	0.99913	19.47788	20.75135	21.07749
EMBR3	3.91241	4.05584	4.06086	0.99502	1.00003	0.99934	15.33249	16.58893	16.64500
JBSS3	4.05243	4.12806	4.14665	0.99953	0.99995	0.99738	16.43317	17.18593	17.35383
SUZB3	4.21111	4.27896	4.31075	0.99986	1.00013	0.99900	17.75711	18.42779	18.71943
BPAC11	3.91545	4.13931	4.16770	0.98401	1.00007	0.99891	15.36805	17.77130	18.02920
EQTL3	4.34100	4.31809	4.35359	1.00110	1.00042	0.99827	18.87290	18.76692	19.08392
PRIO3	3.84134	4.07300	4.10679	0.98573	0.99838	0.99885	14.77555	16.73885	17.01305
RENT3	3.89184	4.04533	4.05838	1.00180	1.00018	0.99812	15.15786	16.49800	16.62137
RDOR3	3.73238	3.90752	3.93236	0.97481	0.99973	0.99719	13.96350	15.39790	15.60459
RADL3	4.16646	4.25924	4.28907	0.99791	1.00030	0.99880	17.36874	18.25833	18.53457
BBSE3	4.56255	4.62184	4.64559	0.98890	1.00013	0.99815	20.84392	21.52285	21.73975
GGBR4	4.08127	4.23514	4.26619	0.99317	1.00014	0.99767	16.67891	18.06022	18.34012
RAIL3	4.07208	4.20381	4.23771	0.99057	1.00018	0.99876	16.59762	17.78989	18.08810
CMIG4	4.17938	4.29497	4.32423	0.98634	0.99909	0.99710	17.48242	18.59088	18.88248
BRFS3	3.60834	3.72013	3.73733	0.98985	1.00008	0.99798	13.04872	14.02937	14.18631
ENEV3	4.02871	4.10095	4.13453	0.99439	1.00028	0.99833	16.24903	16.94846	17.23215
VBBR3	3.90299	4.07395	4.10143	0.99382	1.00010	0.99876	15.24786	16.72812	16.96565
VIVT3	4.43015	4.45829	4.48141	0.99993	1.00015	0.99890	19.64682	19.99890	20.21777
KLBN11	4.29551	4.37559	4.40866	0.99067	1.00013	0.99871	18.46167	19.27558	19.56252
UGPA3	3.96155	4.13476	4.15658	0.98993	1.00033	0.99792	15.72370	17.23659	17.42141
BBDC3	4.35775	4.45628	4.47404	0.99154	0.99922	0.99820	19.03886	20.58647	20.34201
CPLE6	4.24355	4.33745	4.37060	0.98477	1.00032	0.99821	18.03001	18.92756	19.22572
TOTS3	3.94505	4.09428	4.11987	0.98932	1.00006	0.99846	15.58403	16.90997	17.13124
LREN3	3.58149	3.77674	3.78949	1.00044	1.00009	0.99795	12.83014	14.38604	14.49967
TIMS3	4.30841	4.36944	4.39373	1.00044	1.00017	0.99854	18.57575	19.38717	19.61237
ENGI11	4.12850	4.22674	4.24516	0.99685	1.00016	0.99861	17.05410	17.99105	18.15812
STBP3	3.83410	4.08969	4.07837	0.93806	0.99433	0.98491	14.81509	17.03139	16.89089
NTCO3	3.60471	3.79837	3.82018	0.97356	0.99993	0.99728	13.03205	14.59597	14.77216
ELET6	4.15501	4.28446	4.32281	0.99045	1.00038	0.99837	17.28776	18.49136	18.84641
HAPV3	3.36925	3.54053	3.56724	0.98430	0.99931	0.99570	11.42847	12.72988	12.93281
CCRO3	4.18785	4.25766	4.30069	0.98897	1.00022	0.99681	17.56276	18.43266	19.16036
CSAN3	3.94281	4.09902	4.11367	1.00039	1.00018	0.99925	15.56055	16.91291	17.05833
EGIE3	4.55261	4.63455	4.65068	0.99678	1.00020	0.99875	20.73179	21.60023	21.76312
SANB11	4.26097	4.46741	4.45860	0.99515	0.99910	0.99895	18.16559	20.63935	20.20357
CMIN3	3.78411	4.05681	4.05288	0.99779	1.00009	0.99839	14.33022	16.60577	16.58056
ASAI3	3.74801	3.76278	3.79175	1.02472	0.99998	1.00064	14.05684	14.29698	14.52837
CXSE3	4.29792	4.40884	4.43203	0.98924	1.00056	0.99949	18.48475	19.59515	19.80687
TAEE11	4.73643	4.85975	4.88262	0.99080	1.00075	1.00017	22.45530	24.32728	24.55431
HYPE3	4.06001	4.13895	4.16003	1.00031	1.00026	0.99985	16.49266	17.27464	17.47054
MULT3	4.07811	4.21972	4.24526	0.98216	1.00036	0.99838	16.66058	17.92932	18.15970
PSSA3	4.39688	4.39307	4.42714	0.99211	1.00034	0.99827	19.36248	19.43120	19.74251
GOAU4	4.14534	4.30513	4.32973	0.99527	1.00006	0.99819	17.20906	18.65908	18.88120
CSNA3	3.71985	4.02745	4.05204	0.98622	0.99997	0.99789	13.87363	16.35841	16.58778
CPFE3	4.34145	4.44226	4.47436	0.97405	1.00008	0.99856	18.88085	19.87943	20.17035
FLRY3	4.11794	4.26239	4.28079	0.98327	0.99998	0.99804	17.01450	18.30443	18.47825
MRFG3	3.70839	3.80340	3.82063	0.99865	1.00016	0.99832	13.76796	14.59875	14.74763
POMO4	3.89349	3.90670	3.92733	1.00231	1.00024	0.99929	15.18542	15.39255	15.56519
RECV3	3.74885	3.95216	3.96224	0.99136	0.99996	0.99838	14.06348	15.75148	15.85764
CYRE3	3.78424	3.93947	3.96947	0.99132	1.00057	0.99901	14.32992	15.63537	15.88446
BRAP4	4.11674	4.49995	4.52336	0.98710	0.99996	0.99851	16.96410	20.35986	20.58671
AZZA3	3.76609	3.87111	3.88914	1.00192	1.00012	0.99897	14.19094	15.10956	15.27138
IGTI11	4.03063	4.14516	4.16868	0.97842	1.00032	0.99843	16.29603	17.29665	17.50372
IRBR3	3.53881	3.71233	3.72331	0.98312	0.99788	0.99715	12.57382	13.98804	14.10229
SLCE3	4.24615	4.26371	4.31619	0.98124	1.00010	0.99925	18.05049	18.32966	18.79468
SMTO3	3.80826	3.96757	3.97741	0.98535	1.00009	0.99793	14.52267	15.86197	15.95135
BRKM5	3.73581	3.83294	3.84394	1.00049	0.99959	0.99864	13.97893	14.84483	14.94474
CRFB3	3.65702	3.77489	3.77303	1.01966	1.00023	1.00029	13.38314	14.37987	14.37792
RAIZ4	3.72872	3.87511	3.89291	0.99217	1.00007	0.99854	13.93099	15.15531	15.31291
USIM5	3.89558	4.11150	4.13229	0.99065	1.00091	1.00033	15.20591	17.07189	17.25607
VIVA3	3.78677	3.90481	3.92642	0.99138	0.99979	0.99813	14.35051	15.36597	15.55092
YDUQ3	3.46596	3.59708	3.59971	0.99613	0.99989	0.99778	12.03796	13.08338	13.11557
MGLU3	3.13415	3.47005	3.44166	0.98754	1.00261	0.99706	9.83080	12.77295	12.23904
VAMO3	3.61876	3.70222	3.71688	0.99879	0.99996	0.99935	13.12387	13.83541	13.97197
COGN3	3.53779	3.61513	3.63651	1.00036	0.99982	0.99823	12.53107	13.19813	13.36922
MRVE3	3.52309	3.62724	3.64474	0.99770	1.00006	0.99905	12.42731	13.29230	13.44458
LWSA3	3.35288	3.60353	3.61256	0.97992	1.00013	0.99764	11.26625	13.12850	13.20464
AZUL4	3.28449	3.45956	3.45625	0.99601	0.99962	0.99785	10.81989	12.13603	12.14149
BEEF3	3.86902	3.93761	3.94900	1.00305	1.00006	0.99801	14.99721	15.65433	15.76750
PCAR3	3.52749	3.58325	3.59065	1.00909	1.00109	1.00200	12.46819	13.01316	13.06843
PETZ3	3.38289	3.57439	3.56063	0.99619	1.00002	0.99617	11.45159	13.51054	13.05632
CVCB3	3.18966	3.44453	3.42717	0.99551	1.00022	0.99440	10.19043	12.57352	12.59192

Note: This table compares forecasting performance across three volatility estimation methods – Stochastic Volatility (SV), OHLC (Open-High-Low-Close), and High-Low range (HL) – using Mean Absolute Error (MAE), Mean Absolute Percentage Error (MAPE) and Mean Squared Error (MSE) for 771 observations.

and HL models, it is 21.91202 and 21.59300, respectively. These results indicate that the SV model generates more accurate forecasts by minimizing large discrepancies between predicted and actual values.

Overall, the analysis of error metrics suggests that integrating the stochastic volatility (SV) model within the FNETS framework significantly improves forecasting performance, consistently producing lower MAE, MAPE, and MSE values. Conversely, the HL model underperforms across nearly all metrics. From an economic perspective, this result can be attributed to the inherent nature of financial markets, which are subject to sudden fluctuations driven by new information, economic shocks, and shifts in investor sentiment. The SV model effectively captures these dynamic, time-varying patterns, making it a more reliable choice for risk management and derivative pricing.

In contrast, the HL model, which relies solely on high and low prices, oversimplifies the complex behavior of market volatility. By disregarding the stochastic nature of volatility clustering and abrupt market movements, it fails to provide accurate forecasts, reinforcing the necessity of employing models that account for the underlying randomness and structural dependencies in financial data.

5. Conclusions

This study integrates Factor Adjusted Network Analysis (FNETS), as proposed by (Barigozzi et al., 2024), with Univariate Stochastic Volatility modeling to analyze volatility interdependencies among 82 Brazilian stocks in the post-pandemic period (January 3, 2022, to January 28, 2025). The selected stocks correspond to the theoretical portfolio composition of the Ibovespa Index for the January–April 2025 period.

The Granger Causal, Partial Correlation (PC), and Long-Run Partial Correlation (LRPC) heatmaps reveal a heterogeneous connectivity structure, where core portfolio constituents exhibit strong interdependencies, while peripheral stocks display weaker direct linkages. The empirical superiority of the stochastic volatility (SV) model within the FNETS framework, evidenced by consistently lower MAE, MAPE, and MSE values compared to the OHLC and HL approaches, demonstrates its effectiveness in capturing latent volatility dynamics and systemic risk propagation.

Methodologically, integrating FNETS with SV-INLA estimation addresses high-dimensionality challenges and mitigates computational inefficiencies commonly associated with conventional volatility modeling frameworks. From a practical standpoint, identifying critical nodes and sectoral clusters provides valuable insights for targeted risk mitigation and portfolio diversification strategies. Moreover, the attenuated connectivity observed in marginal portfolio constituents underscores the vulnerabilities of less-centralized market segments.

These findings enhance crisis monitoring tools for policymakers and refine risk management strategies for investors navigating volatile emerging markets. Future research could extend this framework by incorporating nonlinear dependencies or analyzing the temporal evolution of network structures under systemic shocks.

Acknowledgments

Author One would like to thank Institution One for financial support.

References

Barigozzi, M., Cho, H. and Owens, D. (2024). Fnets: Factor-adjusted network estimation and forecasting for high-dimensional time series, *Journal of Business & Economic Statistics* **42**(3): 890–902.

Basu, S. and Michailidis, G. (2015). Regularized estimation in sparse high-dimensional time series models, *The Annals of Statistics* **43**(4): 1535–1567.

Bostanci, G. and Yilmaz, K. (2020). How connected is the global sovereign credit risk network?, *Journal of Banking & Finance* **113**: 105761.

Brillinger, D. R. (1964). The generalization of the techniques of factor analysis, canonical correlation and principal components to stationary time series. Invited Paper at the Royal Statistical Society Conference in Cardiff, Wales.

Brillinger, D. R. (1981). *Time Series: Data Analysis and Theory*, Classics in Applied Mathematics, Society for Industrial and Applied Mathematics.

Cai, T., Liu, W. and Luo, X. (2011). A constrained l 1 minimization approach to sparse precision matrix estimation, *Journal of the American Statistical Association* **106**(494): 594–607.

Chaim, P. and Laurini, M. P. (2024). Bayesian inference for long memory stochastic volatility models, *Econometrics* **12**(4).
URL: `https://www.mdpi.com/2225-1146/12/4/35`

Cotter, J., Hallam, M. and Yilmaz, K. (2023). Macro-financial spillovers, *Journal of International Money and Finance* **133**: 102824.

de Zea Bermudez, P., Marín, J. M., Rue, H. and Veiga, H. (2024). Integrated nested laplace approximations for threshold stochastic volatility models, *Econometrics and Statistics* **30**: 15–35.
URL: https://www.sciencedirect.com/science/article/pii/S2452306221001003

Demirer, M., Diebold, F. X., Liu, L. and Yilmaz, K. (2018). Estimating global bank network connectedness, *Journal of Applied Econometrics* **33**(1): 1–15.

Demirer, M., Gokcen, U. and Yilmaz, K. (2019). Financial sector volatility connectedness and equity returns, *Working Paper 3099738*, SSRN.
URL: https://ssrn.com/abstract=3099738

Diebold, F. X. and Yilmaz, K. (2009). Measuring financial asset return and volatility spillovers, with application to global equity markets, *The Economic Journal* **119**(534): 158–171.

Diebold, F. X. and Yilmaz, K. (2011). Equity Market Spillovers in the Americas, *in* R. Alfaro (ed.), *Financial Stability, Monetary Policy, and Central Banking*, Vol. 15 of *Central Banking, Analysis, and Economic Policies Book Series*, Central Bank of Chile, chapter 7, pp. 199–214.
URL: https://ideas.repec.org/h/chb/bcchsb/v15c07pp000-000.html

Diebold, F. X. and Yilmaz, K. (2012). Better to give than to receive: Predictive directional measurement of volatility spillovers, *International Journal of Forecasting* **28**(1): 57–66.

Diebold, F. X. and Yılmaz, K. (2014). On the network topology of variance decompositions: Measuring the connectedness of financial firms, *Journal of Econometrics* **182**(1): 119–134.

Diebold, F. X. and Yilmaz, K. (2015). Trans-atlantic equity volatility connectedness: US and European financial institutions, 2004–2014, *Journal of Financial Econometrics* **14**(1): 81–127.

Ehlers, R. and Zevallos, M. (2015). Bayesian estimation and prediction of stochastic volatility models via INLA, *Communications in Statistics - Simulation and Computation* **44**(3): 683–693.

Forni, M., Hallin, M., Lippi, M. and Reichlin, L. (2000). The generalized dynamic-factor model: Identification and estimation, *Review of Economics and Statistics* **82**(4): 540–554.

Forni, M. and Lippi, M. (2001). The generalized dynamic factor model: Representation theory, *Econometric Theory* **17**(6): 1113–1141.

Garman, M. B. and Klass, M. J. (1980). On the estimation of security price volatilities from historical data, *Journal of Business* pp. 67–78.

Hansen, P. R. and Lunde, A. (2006). Realized variance and market microstructure noise, *Journal of Business & Economic Statistics* **24**(2): 127–161.
URL: https://doi.org/10.1198/073500106000000071

Kock, A. B. and Callot, L. (2015). Oracle inequalities for high dimensional vector autoregressions, *Journal of Econometrics* **186**(2): 325–344.

Korobilis, D. and Yilmaz, K. (2018). Measuring Dynamic Connectedness with Large Bayesian VAR Models, *Essex Finance Centre Working Papers 20937*, University of Essex, Essex Business School.
URL: https://ideas.repec.org/p/esy/uefcwp/20937.html

Laurini, M., Nacinben, J. P. C. d. S. M., Franco, J. P. M. and Chaim, P. (2024). A multivariate stochastic volatility model with generalized factor dynamics, *Technical report*, SSRN.
URL: https://ssrn.com/abstract=4913625

Martino, S. (2007). Approximate Bayesian inference for multivariate stochastic volatility models, *Technical report*, Citeseer.

Martino, S., Aas, K., Lindqvist, O., Neef, L. R. and Rue, H. (2011). Estimating stochastic volatility models using integrated nested Laplace approximations, *The European Journal of Finance* **17**(7): 487–503.

Masini, R. P., Medeiros, M. C. and Mendes, E. F. (2022). Regularized estimation of high-dimensional vector autoregressions with weakly dependent innovations, *Journal of Time Series Analysis* **43**(4): 532–557.

Nacinben, J. P. C. d. S. M. and Laurini, M. (2024). Multivariate stochastic volatility modeling via integrated nested Laplace approximations: A multifactor extension, *Econometrics* **12**(1): 5.

Niekerk, J. V., Bakka, H., Rue, H. and Schenk, O. (2019). New frontiers in bayesian modeling using the INLA package in r, *Preprint arXiv:1907.10426*, arXiv.
URL: https://arxiv.org/abs/1907.10426

Parkinson, M. (1980). The extreme value method for estimating the variance of the rate of return, *Journal of Business* pp. 61–65.

Rue, H. and Held, L. (2005). *Gaussian Markov random fields: Theory and applications*, Chapman and Hall/CRC.

Rue, H., Martino, S. and Chopin, N. (2009). Approximate Bayesian inference for latent Gaussian models by using integrated nested laplace approximations, *Journal of the Royal Statistical Society Series B: Statistical Methodology* **71**(2): 319–392.

Shapovalova, Y. (2021). "exact" and approximate methods for Bayesian inference: Stochastic volatility case study, *Entropy* **23**(4): 466.

Simpson, D., Rue, H., Riebler, A., Martins, T. G. and Sørbye, S. H. (2017). Penalising model component complexity: A principled, practical approach to constructing priors.

Taylor, S. J. (1982). Financial returns modelled by the product of two stochastic processes-a study of the daily sugar prices 1961-75, *Time series analysis: Theory and practice* **1**: 203–226.

Wong, K. C., Li, Z. and Tewari, A. (2020). Lasso guarantees for β-mixing heavy-tailed time series, *The Annals of Statistics* **48**(2): 1124–1142.

Yilmaz, K. (2010). Return and volatility spillovers among the East Asian equity markets, *Journal of Asian Economics* **21**(3): 304–313.

Zhang, W.-G., Mo, G.-L., Liu, F. and Liu, Y.-J. (2018). Value-at-risk forecasts by dynamic spatial panel GJR-GARCH model for international stock indices portfolio, *Soft Computing* **22**: 5279–5297.

A. Fnets Assumptions

Consider the spectral density matrices of the processes $\boldsymbol{X}_t$, $\boldsymbol{\chi}_t$, and $\boldsymbol{\xi}_t$ at frequency $\omega \in [-\pi, \pi]$, denoted respectively by $\boldsymbol{\Sigma}_x(\omega)$, $\boldsymbol{\Sigma}_\chi(\omega)$, and $\boldsymbol{\Sigma}_\xi(\omega)$. Let $\mu_{x,j}(\omega)$, $\mu_{\chi,j}(\omega)$, and $\mu_{\xi,j}(\omega)$ (for $j \geqslant 1$) represent the corresponding dynamic eigenvalues associated with $\boldsymbol{X}_t$, $\boldsymbol{\chi}_t$, and $\boldsymbol{\xi}_t$, respectively.

Assumption 1. There exists a positive integer $p_0 \geqslant 1$, constants $\rho_j \in (3/4, 1]$ with $\rho_1 \geqslant \ldots \geqslant \rho_q$, and pairs of continuous functions $\omega \mapsto \alpha_{\chi,j}(\omega)$ and $\omega \mapsto \beta_{\chi,j}(\omega)$ for $\omega \in [-\pi, \pi]$ and $1 \leqslant j \leqslant q$, such that for all $p \geqslant p_0$,

$$\begin{aligned} \beta_{\chi,1}(\omega) \geqslant \frac{\mu_{\chi,1}(\omega)}{p^{\rho_1}} &\geqslant \alpha_{\chi,1}(\omega) > \cdots > \beta_{\chi,q}(\omega) \\ \geqslant \frac{\mu_{\chi,q}(\omega)}{p^{\rho_q}} &\geqslant \alpha_{\chi,q}(\omega) > 0. \end{aligned}$$

If $\rho_j = 1$, for all $1 \leqslant j \leqslant q$, then, by Assumption 1, we have q common factors, which are equally pervasive for the entire cross-section. However, if $\rho_j < 1$, for some j, the presence of "weak" common factors is allowed and, in this case, as outlined in Barigozzi et al. (2024), the ordering of the variables becomes more important as $p \to \infty$. Furthermore, it is important to note that when the dimensionality increases and heavy tails are included in the problem, larger values for ρ_j are required.

Assumption 2. There exist some constant $\Xi > 0$ and $\varsigma > 2$, such that for all $l \geqslant 0$,

$$\max_{1 \leqslant i \leqslant p} |\boldsymbol{B}_{l,i\cdot}|_2 \leqslant \Xi(1+l)^{-\varsigma} \quad \text{and}$$
$$\left(\sum_{j=1}^{q} |\boldsymbol{B}_{l,\cdot j}|_\infty^2 \right)^{1/2} \leqslant \Xi(1+l)^{-\varsigma}.$$

Assumption 3.
1. d is a finite positive integer and $det(\mathscr{A}(z)) \neq 0$ for all $|z| \leqslant 1$;
2. There exist some constants $0 < m_\varepsilon < M_\varepsilon$ such that $\|\Gamma\| \leqslant M_\varepsilon$ and $\Lambda_{min}(\Gamma) \geqslant m_\varepsilon$;
3. There exist a constant $m_\xi > 0$ such that $\inf_{\omega \in [-\pi,\pi]} \mu_{\xi,p}(\omega) \geqslant m_\xi$;

4. There exist some constants $\Xi > 0$ and $\varsigma > 2$ such that for all $l \geqslant 0$,

$$|D_{l,ik}| \leqslant C_{ik}(1+l)^{-\varsigma} \quad \text{with}$$
$$\max\left\{\max_{1\leqslant k\leqslant p}\sum_{i=1}^{p} C_{ik},\ \max_{1\leqslant i\leqslant p}\sum_{k=1}^{p} C_{ik},\ \max_{1\leqslant i\leqslant p}\sqrt{\sum_{k=1}^{p} C_{ik}^2}\right\}\leqslant \Xi.$$

Barigozzi et al. (2024) emphasizes that, by Assumptions 2 and 3 (*4*), the Wold decomposition can be impose on the idiosyncratic component equation and, therefore, the serial dependence present in $\boldsymbol{X}_t$ decays at an algebraic rate.

Proposition 1. Under Assumption 3, uniformly over all $\omega \in [-\pi, \pi]$, there exists some constant $B_\xi > 0$ depending only on M_ε and ς, defined in Assumption 3 (*3*) and (*4*), such that $\sup_{\omega\in[-\pi,\pi]} \mu_{\xi,1}(\omega) \leqslant B_\xi$.

Remark 1. Proposition 1 and Assumption 3 (*3*) jointly establish the uniform boundedness of $\mu_{\xi,1}(\omega)$ and $\mu_{\xi,p}(\omega)$, which is commonly assumed in the literature on high-dimensional VAR estimation via l_1-regularization. A sufficient condition for Assumption 3 (*3*) is that

$$\max\left\{\max_{1\leqslant i\leqslant p}\sum_{l=1}^{d} |\boldsymbol{A}_{l,i\cdot}|_1,\ \max_{1\leqslant j\leqslant p}\sum_{l=1}^{d} |\boldsymbol{A}_{l,\cdot j}|_1\right\}\leqslant \Xi$$

for some constant $\Xi > 0$ (Basu and Michailidis, 2015). Further, when for example, $d = 1$, Assumption 3 (*4*) follows if $|\boldsymbol{A}_1|_\infty \leqslant \gamma < 1$ since $\max(\|\boldsymbol{D}_l\|_1, \|\boldsymbol{D}_l\|_\infty) \leqslant \Xi\gamma^l$, with $\boldsymbol{D}_l = \boldsymbol{A}_1^l$.

Barigozzi et al. (2024) argues that the identification of the latent components, $\boldsymbol{\chi}_t$ and $\boldsymbol{\xi}_t$, and also the number of common factors q, is possible due to the large difference between the eigenvalues of their spectral density matrices[†]. Therefore, using the Weyl´s inequality, the qth dynamic eigenvalue, denote as $\mu_{x,q}(\omega)$, diverges almost everywhere (a.e.) in $[-\pi, \pi]$ as $p \to \infty$, while the $q+1$th dynamic eigenvalue, $\mu_{x,q+1}(\omega)$, is uniformly bounded for any ω and $p \in \mathbb{N}$.

Assumption 4. 1. $\{\boldsymbol{u}_t\}_{t\in\mathbb{Z}}$ is a sequence of zero-mean, q-dimensional martingale difference vectors with $Cov[\boldsymbol{u}_t] = \boldsymbol{I}_q$, and u_{it} and u_{jt} are independent for all $1 \leqslant i, j \leqslant q$ with $i \neq j$ and all $t \in \mathbb{Z}$;

[†] This result derives from Assumption 1 and Proposition 1.

2. $\{\boldsymbol{\varepsilon}_t\}_{t\in\mathbb{Z}}$ is a sequence of zero-mean, p-dimensional martingale difference vectors with $Cov[\boldsymbol{\varepsilon}_t] = \boldsymbol{I}_p$, and ε_{it} and ε_{jt} are independent for all $1 \leqslant i, j \leqslant p$ with $i \neq j$ and all $t \in \mathbb{Z}$;

3. $E[u_{jt}\varepsilon_{it'}] = 0$ for all $1 \leqslant j \leqslant q$, $1 \leqslant i \leqslant p$ and $t, t' \in \mathbb{Z}$;

4. There exist some constant $\nu > 4$ and $\mu_\nu > 0$ such that $\max\{\max_{1\leqslant j\leqslant q} E[|u_{jt}|^\nu], \max_{1\leqslant i\leqslant p} E[|\varepsilon_{it}|^\nu]\} \leqslant \mu_\nu$.

The Assumption 4 describes the characteristics of innovations for common and idiosyncratic estimates. According to Barigozzi et al. (2024), Assumption 4 (*1*) and (*2*) enable the common and idiosyncratic innovations to be carried out as martingale differences sequences. By Assumption (4.*4*), the innovations must have $\nu > 4$ moments, which is significantly weaker than the Gaussian or sub-Weibull tails typically assumed in the high-dimensional time series VAR modeling literature (Basu and Michailidis, 2015; Kock and Callot, 2015; Wong et al., 2020; Masini et al., 2022).